Title

Cardiac MRI: a Translational Imaging Tool for Characterizing Anthracycline-Induced Myocardial Remodeling

Journal

Current Oncology Reports, 18(8)

ISSN

1523-3790

Authors

Nguyen, Kim-Lien
Hu, Peng
Ennis, Daniel B
et al.

Publication Date

2016-08-01

DOI

10.1007/s11912-016-0533-x

Peer reviewed

Curr Oncol Rep (2016) 18: 48
DOI 10.1007/s11912-016-0533-x

Cardiac MRI: a Translational Imaging Tool for Characterizing Anthracycline-Induced Myocardial Remodeling

Kim-Lien Nguyen[1,2] · **Peng Hu**[1,3] · **Daniel B. Ennis**[3] · **Jiaxin Shao**[1,3] · **Kimberly A. Pham**[2] · **Joseph J. Chen**[2]

Published online: 13 June 2016

Abstract Cardiovascular side effects of cancer therapeutics are the leading causes of morbidity and mortality in cancer survivors. Anthracyclines (AC) serve as the backbone of many anti-cancer treatment strategies, but dose-dependent myocardial injury limits their use. Cumulative AC exposure can disrupt the dynamic equilibrium of the myocardial microarchitecture while repeated injury and repair leads to myocyte loss, interstitial myocardial fibrosis, and impaired contractility. Although children are assumed to have greater myocardial plasticity, AC exposure at a younger age portends worse prognosis. In older patients, there is lower overall survival once they develop cardiovascular disease. Because aberrations in the myocardial architecture predispose the heart to a decline in function, early detection with sensitive imaging tools is crucial and the implications for resource utilization are substantial. As a comprehensive imaging modality, cardiac magnetic resonance (CMR) imaging is able to go beyond quantification of ejection fraction and myocardial deformation to characterize adaptive microstructural and microvascular changes that are important to myocardial tissue health. Herein, we describe CMR as an established translational imaging tool that can be used clinically to characterize AC-associated myocardial remodeling.

Keywords Cardiac magnetic resonance imaging · Cardiotoxicity · Cardio-oncology · Anthracyclines · Translational imaging

This article is part of the Topical Collection on *Cardio-oncology*

Kimberly A. Pham and Joseph J. Chen contributed equally to this work.

✉ Kim-Lien Nguyen
klnguyen@ucla.edu

[1] Diagnostic Cardiovascular Imaging Laboratory, David Geffen School of Medicine at UCLA and VA Greater Los Angeles Healthcare System, Los Angeles, CA, USA

[2] Division of Cardiology, David Geffen School of Medicine at UCLA and VA Greater Los Angeles Healthcare System, 11301 Wilshire Blvd, MC 111E, Los Angeles, CA 90024, USA

[3] Department of Radiological Sciences, David Geffen School of Medicine at UCLA, Los Angeles, CA, USA

Introduction

Chemotherapy enables cancer patients to survive longer. As a result, many patients face unintended and off-target consequences of cancer treatment. While cardiotoxicity encompasses a host of side effects related to cancer therapy, herein, cardiotoxicity refers to myocardial injury, which may lead to heart failure with preserved or reduced ejection fraction (HFpEF, HFrEF). Both forms of heart failure are associated with increased morbidity and mortality [1••]. Of the various cancer therapies, anthracyclines (AC) represent one of the most effective classes of anti-cancer agents often used in the treatment of leukemias, sarcomas, and lymphomas. However, AC can disrupt normal cell function and lead to adverse remodeling of the myocardial extracellular matrix (ECM) [2, 3•, 4]. Cycles of repeated injury and repair of the ECM can contribute to irreversible and clinically important myocardial dysfunction [4, 5]. Based on published guidelines of the American College of Cardiology/American Heart Association (ACC/AHA), asymptomatic cardiac morphologic change heralds potential heart failure, which is a progressive disorder whereby the transition period from asymptomatic structural abnormalities (stage B) to the development of overt symptoms (stage C or D) may be variable [6]. In spite of cardiovascular (CV) side effects, cancer therapy is often necessary and life changing. Therefore, collaborative care plans

that incorporate comprehensive imaging tools, such as cardiovascular magnetic resonance [CMR] imaging, may potentially improve patient-centered care through earlier detection of myocardial abnormalities.

The goal of this paper is to equip clinicians caring for cancer patients and survivors with knowledge about the role of CMR-derived quantitative measures of myocardial health. The myocardial ECM and its influence on remodeling will be summarized. Additionally, relevant CMR pulse sequences (i.e., different ways of encoding diagnostic information in CMR images) and clinical studies using CMR will be discussed.

The Natural History of Cardiotoxicity

The natural history of chemo-induced myocardial injury in humans remains incompletely understood. However, available histologic data suggest that myocyte loss is accompanied by ventricular chamber dilation, myocardial edema, and interstitial myocardial fibrosis in the context of less robust regenerative capacity [7–10]. Based on clinical studies, AC-induced cardiotoxicity can be separated into three chronological categories: (1) acute, (2) early-onset, and (3) late-onset [5, 11–13]. Acute cardiotoxicity, the least common, occurs immediately after AC infusions and can involve a decline in myocardial contractility [3•, 5, 11–13]. Early-onset cardiotoxicity occurs within a few weeks to a year after exposure and leads to compensatory thickening of the left ventricular (LV) wall termed "adaptive hypertrophy" [3•, 5, 12]. Late-onset cardiotoxicity occurs at least 1 year after exposure but may not become clinically evident until 10–20 years after initial chemotherapy infusion [5, 11]. Those at highest risk of heart failure include exposure to AC dose ≥250 mg/m^2, chest radiation dose ≥35 Gy, or a combination of AC and chest radiation dose ≥100 mg/m^2 (AC) and ≥15 Gy (radiation) [14••].

The Cardiac ECM and Cardiotoxicity: Where Phenotypic Plasticity Relates to Form and Function

The cardiac ECM is an intricate and dynamic network consisting of structural and nonstructural proteins, which provide strength and support to neighboring myocytes. Fluid equilibrium is vital to the overall plasticity of the ECM. Within the myocardial milieu also lies the microvasculature, which provides oxygenation and nutrients that are vital to the overall function of the myocardium. Collagen makes up the bulk of the ECM composition and provides structural integrity. Environmental stress to the myocardium modifies the dynamic relationship between the ECM composition and myocytes, and it is the delicate balance in the up- or down-regulation of fibroblast-mediated collagen turnover that leads to structural remodeling. If collagen synthesis exceeds collagen degradation, the accumulation of collagen in the interstitium results in fibrosis. Although fibrosis as a repair mechanism serves to preserve structural integrity, the scar tissue that forms increases myocardial stiffness and is manifested as diastolic abnormalities [15, 16]. On the other hand, excessive collagen degradation can compromise the integrity of the collagen scaffold and decrease the matrix tensile strength. Changes in ventricular geometry then ensue with wall thinning, ventricular dilation, and eventually systolic dysfunction due to persistent remodeling of the collagen network and further aberrations of the overall myocardial architecture [3•, 16–18].

In the context of AC-induced ECM remodeling, it is important to note that mechanisms associated with AC-induced cardiac injury (topoisomerase 2B mediated) are different from AC treatment effects (topoisomerase 2A mediated) [2]. AC-induced ECM remodeling can occur through several molecular mechanisms [19–21] (Fig. 1). The end result is cellular damage and apoptosis that is reflected by myofibrillar disarray and vacuolization. Because the primary structural role of the ECM is to provide a scaffold for myofiber alignment, recurrent cycles of injury and repair eventually exceed compensatory mechanisms and result in diastolic and systolic abnormalities including both impaired contractile function and filling.

CMR Techniques for Assessment of Myocardial Remodeling

Several comprehensive papers summarizing the general principles of CMR have been published [22–24]. Briefly, CMR leverages the differences in tissue magnetic properties (T1, T2, T2* relaxation time constants) to generate soft-tissue contrast (Fig. 2) and to discriminate between normal and pathologic states [25]. In-plane spatial resolution of 1–2 mm (and sometimes sub millimeter) and temporal resolution of 25–50 ms are typically achievable. By manipulating pulse sequence parameters to generate different types of tissue contrast, CMR provides insight into morphology (volumetry, mass), global and regional function (deformation /strain, ejection fraction [EF]), tissue composition (edema, fibrosis, fat, hemorrhage), and perfusion—all of which could aid in the understanding of AC-induced myocardial remodeling. Although not all components are routinely performed in one single examination, these approaches can be combined and tailored to characterize different aspects of heart health. In stage B of heart failure, any combination or all of these components can be abnormal. Table 1 provides a summary of relevant CMR techniques while Tables 2 and 3 summarize clinical studies relating to CMR and AC-associated CV remodeling.

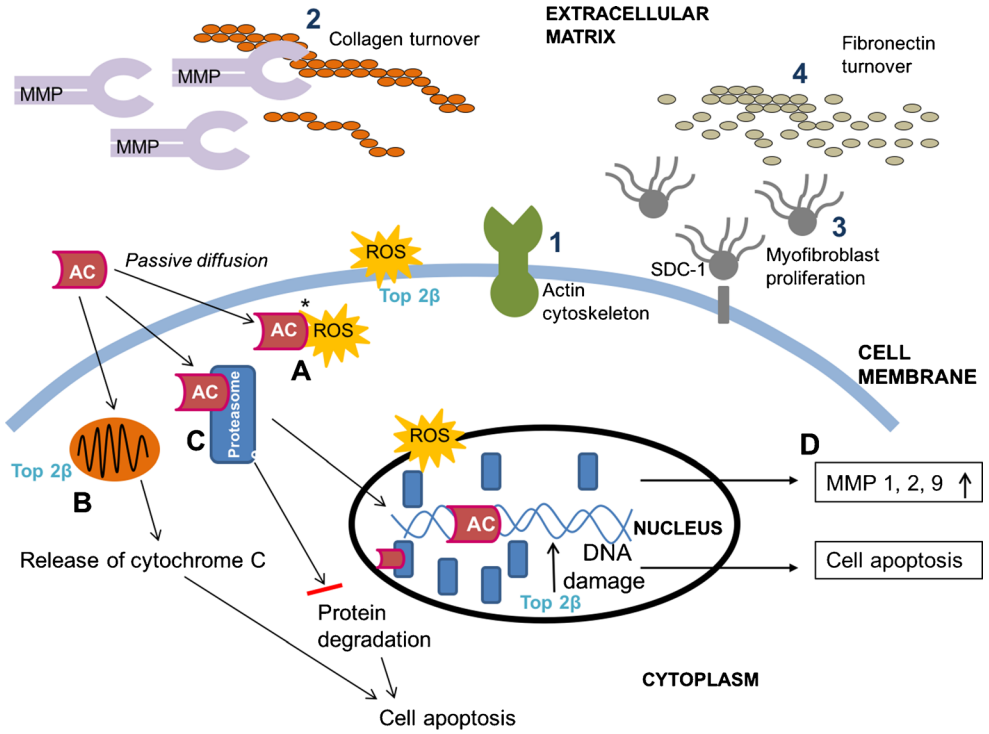

Fig. 1 Anthracycline-associated myocyte damage (*A–D*) and extracellular matrix remodeling (*1–4*). Topoisomerase 2B is the primary mediator of AC-induced cardiotoxicity and causes direct ds-DNA breakage, impaired mitochondrial biogenesis, and ROS production. AC passively diffuses into the myocyte to trigger signaling pathways of myocardial injury and repair. Iron-anthracycline complexes cause ROS generation, which leads to lipid peroxidation and membrane damage (*A*). In the mitochondrion, DOX-induced ROS causes release of cytochrome C leading to cell death (*B*). AC binds to proteasomes with high affinity and translocate into the nucleus to intercalate into DNA (*C*). As DNA damage increases, apoptosis pathways are activated. Increased cellular stress by ROS generation leads to increased MMP expression (*D*). Compensatory ECM remodeling is reflected as (*1*) actin cytoskeleton activity at the cell-ECM interface, (*2*) MMP-induced collagen breakdown and turnover which can lead to fibrosis (scar) formation, (*3*) myofibroblast proliferation to increase matrix protein (fibronectin) deposition secondary to SDC-1 shedding, and (*4*) cystatin C/cathepsin-mediated fibronectin turnover. *AC* anthracycline, *ds* double-stranded, *ECM* extracellular matrix, *MMP* matrix metalloproteinase, *ROS* reactive oxygen species, *SDC-1* syndecan-1, *Top 2β* topoisomerase 2 β. Adapted from Nikitovic D, Juranek I, Wilks MF, Tzardi M, Tsatsakis A, Tzanakakis GN. Anthracycline-dependent cardiotoxicity and extracellular matrix remodeling. Chest. 2014;146(4):1123–30. doi:10.1378/chest.14-0460, with permission from Elsevier

Cardiac Cine and Myocardial Tagging for Morphology and Function

Segmented cine balanced steady state free precession (bSSFP) is widely used to acquire dynamic "movies" of the beating heart termed "cardiac cine imaging." The EF, volumetry, and mass are then quantified without the need for geometric assumptions or incomplete sampling of cardiac chamber volumes [25–28] (Fig. 2a). The left ventricular ejection fraction (LVEF) is a widely used index to monitor for cardiac dysfunction and can be measured using echocardiography, CMR, and several other imaging modalities. While echo is widely available and cost-effective [29], overestimation of EF using 2D echo (2DE) and 3D echo (3DE) has been described in adult survivors of childhood cancer [30, 31] (Table 2). The 2DE false-negative rate is 75 % while the 3DE false-negative rate is 47 % for detection of EF less than 50 % [30]. CMR is superior to 2DE for quantification of EF with high inter-study reproducibility (coefficient of variability 2.4–7.3 % [EF], 2.8–4.8 % [mass], $p < 0.001$) [32, 33].

It is instructive to note that lower right ventricular EF has been reported in a cross-sectional cohort of childhood cancer survivors [34, 35], while in adult cancer survivors, lower LVEF and aortic stiffness persisted at 14 months post-AC exposure [36] (Table 2). In adult survivors with HFrEF, CMR-derived LV mass index predicted major adverse cardiac events (MACE) [37]. Importantly, preliminary findings suggest that in those already taking statins during AC exposure, there is no significant decline in LVEF [38]. While the cohort was small, the findings are informative in light of reports by Cardinal et al.: in 207 AC-induced cardiomyopathy patients with and without symptoms of heart failure, 42 % did not recover their LVEF with enalapril and carvedilol [39]. Because treatment implications still rely predominantly on the LVEF, accurate quantification and reproducibility is vital for the longitudinal care of patients. In this regard, CMR remains the gold standard for accurate and reproducible quantification of biventricular EF [40] and the majority of published work in the area of CMR and cardio-oncology has focused on inter-modality comparisons of EF (Table 2).

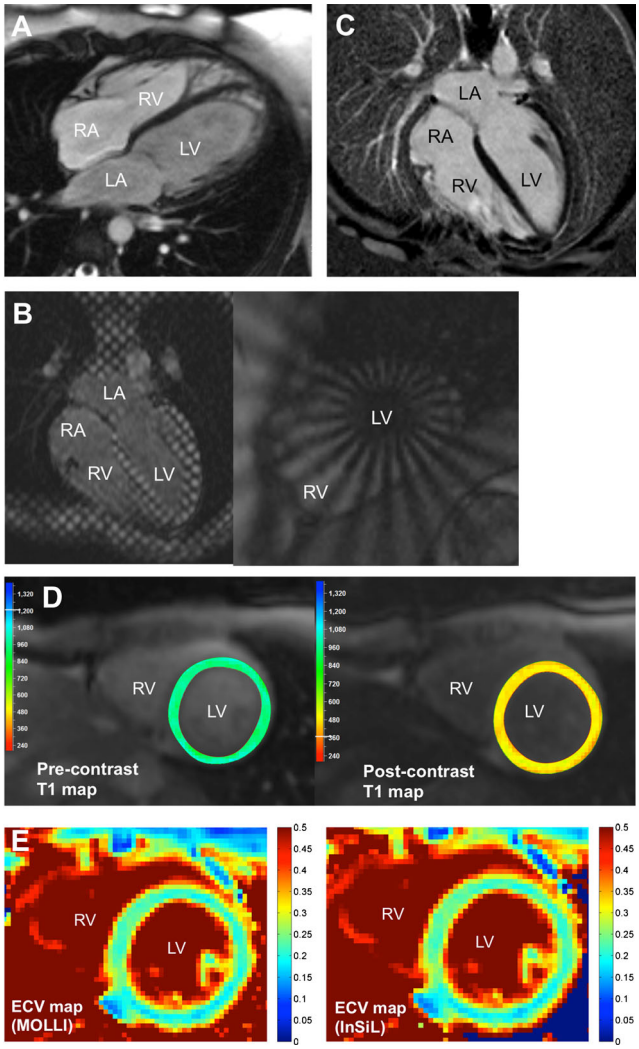

Fig. 2 Comprehensive CMR imaging (1.5 T) of a 33-year-old male with anthracycline exposure at age 12. **a** Morphologic myocardial characterization using cardiac cine imaging (end-diastolic frame) demonstrates reduced left ventricular mass (myocyte loss), ventricular dilation, increased ventricular trabeculation, but normal left ventricular and right ventricular ejection fraction. **b** Myocardial tagging can be performed using conventional Cartesian grid tags (*left*) or radial polar tags (*right*). **c** Late gadolinium enhancement imaging demonstrates no regional fibrosis. **d** Pre-contrast T1 map (*left*, average T1 970 ms) and post-contrast (*right*, average T1 471 ms) using MOLLI were performed. **e** ECV maps using MOLLI (*left*, ECV 0.22 ± 0.02) and InSiL (*right*, ECV 0.22 ± 0.03) demonstrate no diffuse fibrosis. InSiL [100] is a modified T1 mapping algorithm that allows for improved estimation of T1 time with less heart rate dependence. ECV reference range 0.23–0.32 (based on MOLLI). *ECV* extracellular volume fraction, *InSiL* instantaneous signal loss simulation, *MOLLI* modified Look-Locker inversion recovery, *SSFP* steady-state free precession

In recent years, however, several organizations have supported the use of myocardial deformation in the care of patients exposed to cancer therapy [1••, 41••]. Compared to the EF, myocardial deformation is a more sensitive measure of the overall myocardial function because it directly reflects the motion of the myofibers and can be described by both strain and rotational mechanics.

Myocardial tagging allows tracking of myocardial tissue motion through the placement of "tags" (Fig. 2b). Tags are thin lines of reduced signal intensity that appear dark on acquired images and are created using selective radiofrequency saturation pulses [42]. These bands of dark tissue are created within a few milliseconds and can subsequently be observed to deform with the underlying cardiac motion (Fig. 2b). The most widely available sequence for myocardial tagging is spatial modulation of magnetization (SPAMM) [43], which allows tags to be placed in orthogonal directions to form a grid. The tag lines and the intersections of the gridlines serve as "markers" for tissue tracking and deformation can be analyzed using several commercially available software packages. Other techniques of tagging include polar tags [44] and complementary radial tags [45] (Fig. 2b, right panel). Recently, Feature Tracking was developed [46, 47]. This technique uses already acquired cardiac cine images and tracks the endocardial and epicardial borders of the myocardium to generate information on myocardial deformation. While convenient and values obtained from Feature Tracking in small study cohorts have shown promise, further validation is needed.

Myocardial deformation in cancer patients and survivors has been assessed using CMR (Tables 2 and 3). Of note, Drafts et al. [48] conducted a prospective cohort study in adult cancer patients (age range 19–80 years, mean 50 ± 2 years) who were exposed to low and moderate doses of AC for the first time and without radiation therapy. CMR measures, biochemical, and quality of life (QOL) markers were assessed in a double-blinded fashion. The study demonstrated a decline in midwall myocardial circumferential strain (a surrogate for myofiber strain) during early therapy and in the setting of low to moderate dose of AC. Impaired strain was associated with a decline in LVEF that persisted at 6-month follow-up time. Notably, there was a trend toward positive association between abnormal deformation and QOL assessment based on the Minnesota Living with Heart Failure Questionnaire ($r = 0.24$, $p = 0.17$). However, QOL deterioration was significantly associated with AC exposure at low to moderate AC doses ($p = 0.008$). These preliminary findings are instructive and counter past observations that myocardial injury occurs at higher doses of AC (>500 mg/m^2).

Edema and Fibrosis Imaging for Myocardial Composition

Overall cardiac function is a reflection of underlying myocardial tissue health. Because aberrations in myocardial composition correlate well with changes in tissue magnetic

Table 1 Summary of CMR techniques

Clinical information	Category of CMR technique	Commonly used pulse sequences[a]
Morphology and function		
Volumetry, mass, ejection fraction	Cine imaging	Balanced steady-state free precession (bSSFP) at 1.5 T
		Spoiled gradient echo sequences (alternative choice) at 3.0 T
Myocardial deformation	Tagging	Cartesian grid tags (SPAMM or C-SPAMM)
Myocardial composition		
Inflammation	Edema imaging[c]	T2 weighted: black blood (T2w STIR) or bright blood (T2 prepared SSFP; TSE-SSFP hybrid)
		T2 mapping: T2 prepared SSFP
Diffuse fibrosis	T1 mapping or extracellular volume fraction (ECV)[b]	MOLLI
Focal fibrosis	Late gadolinium enhancement imaging	Inversion recovery GRE or SSFP
		PSIR
		Single-shot with SSFP readout
Myocardial perfusion reserve (epicardial coronary and microvascular perfusion)	Stress perfusion imaging	Saturation recovery imaging with GRE-EPI, GRE, or SSFP readout

The reader is directed to Kramer et al. J Cardiovasc Magn Reson. 2013 Oct 8;15:91 for additional detail

bSSFP balanced steady-state free precession, *C-SPAMM* complementary spatial modulation of magnetization, *GRE* gradient echo, *EPI* echo planar imaging, *MOLLI* modified Look-Locker inversion recovery, *PSIR* phase-sensitive inversion recovery, *SPAMM* spatial modulation of magnetization, *STIR* short tau inversion recovery, *TSE* turbo spin echo

[a] Pulse sequence refers to the way in which magnetic resonance data are encoded to produce images

[b] The area of CMR myocardial tissue characterization continues to evolve rapidly and different pulse sequences are available on different vendor platforms. Protocols and normal values may vary based on institutional protocols and vendor. Discussion with local imagers is important

properties, the relaxation time constants (T1 or T2) can be "weighed" to characterize certain aspects of myocardial tissue. Both T1 and T2 are sensitive to the presence of increased water content and collagen [49]. However, T2-weighted (T2w) imaging has been preferentially used for imaging myocardial edema in the setting of acute myocardial injury because prior research supported a higher linear correlation between T2 and water content [50]. T2 imaging approaches include dark-blood vs. bright-blood T2w imaging and quantitative T2 mapping.

Conventional T2 dark-blood imaging relies on pulse sequences that are designed to null the signal of flowing blood while maintaining a high signal in the surrounding stationary tissue [51]. Thus, the region of blood flow appears dark relative to the surrounding bright tissue, which allows for anatomic assessment of the endocardial border and vascular structures. However, this technique can be prone to image artifacts due to bulk motion and /or blood stasis at the LV wall resulting in subendocardial bright rim artifacts [52]. Further, T2w images are non-quantitative. Alternatives to T2w dark-blood imaging are variations of bright-blood T2 techniques [52–54]. Bright-blood T2-prepared, single-shot bSSFP (T2prep bSSFP) imaging can overcome the limitations of T2 dark blood image artifacts [53] and can be used for quantitative T2 mapping, which has lower inter-observer variability because the maps are generated without subjective interpretation by the reading physician [54–56]. Additionally, single shot T2prep bSSFP can be performed during free breathing, which is ideal for patients with reduced respiratory function.

Variants of these T2 techniques have been used to discriminate between acute vs. chronic myocardial injury in settings of myocardial infarction [53, 57, 58] and acute myocarditis [55, 59]. To date, however, there are limited clinical investigations [37, 60–62] using T2 to detect evidence of edema in subclinical cardiotoxicity (Tables 2 and 3). Of these studies, Tham et al. [60] showed no evidence of myocardial edema using T2 mapping in a cross-sectional analysis of childhood cancer survivors. However, the T2 relaxation time was inversely related to AC-dose and peak VO2max ($r = -0.49$, $p = 0.01$). Another study [37] reported the presence of myocardial edema using T2w imaging in one adult patient who was approximately 7 years (interquartile range 3–8.5) out from AC therapy.

Although published CMR evidence of myocardial edema in AC exposure has been limited, myocardial fibrosis has been described on histology [7–10] and in several published CMR investigations. In general, there are several types of myocardial fibrosis including focal (also termed "regional," "replacement") and diffuse interstitial fibrosis [63]. The standard CMR technique for detection of focal fibrosis such as that observed

Table 2 Clinical studies using CMR to investigate anthracycline-associated myocardial remodeling

Author	Population (*N*, age, Ca)	Treatment[a] (mg/m^2 or Gy)	Time interval[c]	CMR	Findings
Armstrong et al., 2012 [30]	$n = 114$ 38.3 ± 6.3 years Leukemia, lymphoma Osteosarcoma	AC type unknown 117 (0–803) 1–30 Gy ($n = 16$), >30 Gy ($n = 21$)	27.8 years (18.4–38.3)	• Function	GOAL: Use CMR as gold standard to assess reliability of 2D E derived EF in childhood cancer survivors. • 14 % ($n = 16$) had LVEF <50 % by CMR • 2DE (biplane): 25 % sensitivity, 75 % false-negative rate for detection of CMR-derived EF < 50 % • 3DE: 53 % sensitivity, 47 % false-negative rate for detection of CMR-derived EF < 50 %; no difference in mean 3DE vs. CMR-derived LVEF ($p = 0.08$)
Toro-Salazar et al., 2016 [31]	$n = 57$ Median 21 years (10–42) Leukemia, lymphoma Solid tumor	328 (200–600) AC unknown Chest radiation, unspecified dose	9 years (2.4–26.9)	• Function • Deformation	GOAL: Use CMR to assess reliability of echo to identify cardiac dysfunction. • 3DE has 68 % sensitivity; 2DE (biplane) has 46 % sensitivity to detect CMR-derived LVEF <55 % • Lower CMR-derived GCS and GLS compared to controls ($p < 0.001$) • Lower CMR-derived GCS associated w/ chest radiation ($p < 0.001$) • Weak correlation between CMR-derived GLS, AC dose ($r = 0.26$, 0.05), and post-chemo interval ($r = 0.28$, $p < 0.04$)
Ylanen et al., 2013 [34]	$n = 62$ (34 F, 28 M) 14.6 ± 3.2 years Lymphoma Leukemia	F: 224 (108–419) M: 184 (80–416) #DOX equivalent 3.6–12 Gy	F: 7.7 years (4.9–13.6) M: 7.8 years (5.0–18.0)	• Function • Fibrosis (LGE)	GOAL: Cross-sectional evaluation of LV and RV function, and focal fibrosis in childhood cancer survivors • 18 % ($n = 11$) w/ LVEF <45 %; 61 % ($n = 38$) w/ LVEF 45–55 %, $p < 0.001$ 27 % ($n = 17$) w/ RVEF <45 %; 53 % ($n = 33$) w/ RVEF 45–55 %, $p < 0.001$; no LGE in all subjects
Cheung et al., 2015 [35]	$n = 58$ 24.5 ± 4.4 years Leukemia	DOX 204 ± 94 Chest radiation, unspecified dose	16.6 ± 5.8 years	• Function • T2* iron • Fibrosis (LGE)	GOAL: Cross-sectional assessment of myocardial iron, fibrosis, and LV and RV function in young adult cancer survivors • LVEF 45–55 % ($n = 5$), ≥55 % ($n = 53$); RVEF <45 % ($n = 7$), 45–55 % ($n = 20$), ≥55 % ($n = 31$) • No association between LV and RVEF with AC dose ($p > 0.05$) • Negative for myocardial iron overload ($n = 27$). • Positive fibrosis: LV ($n = 5$); RV ($n = 22$); RV insertion site hyper-enhancement
Grover et al.,2015 [36][b]	$n = 27$ 54 ± 11 years Breast cancer	EPI 300–600 DOX 150–300 Chest radiation, unspecified dose	1–14 m	• Function	GOAL: Determine aortic remodeling and cardiac function at baseline, 1, 4, and 14 m post-AC • ↑ PWV in Ao 4 m and 14 m post-tx ($p < 0.01$) • Greater ↓Ao distensibility in AC only grp at 1, 4, and 14 m post-tx ($p < 0.01$) • ↓LVEF at 4 m and persisted at 14 m ($p = 0.001$); none had LVEF <55 % • 4 m post-tx: 27 % ($n = 7$) had ↓LVEF >10 % • 14 m post-tx: 19 % ($n = 5$) had persistent ↓LVEF
Neilan et al., 2012 [37]	$n = 91$ 43 ± 18 years Cancer type undisclosed	276 ± 82 Chest radiation, unspecified dose	88 m (IQR 37 to 138) m	• Structure and function • Edema (T2w) • Fibrosis (LGE)	GOAL: Cross-sectional analysis of LV mass index (LVMi) as predictor of MACE[e] in adult survivors of cancer with rEF AC-CM • LVMi and AC dose were inversely related ($r = -0.67$, $p < 0.001$) • LVMi (<57 mg/m^2) had strongest adjusted association with MACE (100 % sensitivity and 85 % specificity for MACE prediction, HR 0.87, $\chi^2 = 23$, $p < 0.0001$, AUC 0.90 [95 % CI 0.82–0.95]) • T2: $n = 1$ with qualitative and quantitative edema[d]; LGE positive ($n = 5$)

Unless otherwise noted, age is reported as mean ± standard deviation at time of visit. For studies with multiple types of AC, DOX equivalent dosage is reported when available and noted (#)

d day, *2DE* 2D echocardiography, *3DE* 3D echocardiography, *Ao* ascending aorta, *DOX* doxorubicin, *EPI* epirubicin, *GCS* global circumferential strain, *GLS* global longitudinal strain, *m* month, *LA* left atrial, *LGE* late gadolinium enhancement, *LVEF* left ventricular ejection fraction, *LVMi* left ventricular mass index, *MACE* major adverse cardiovascular event, *pEF* preserved ejection fraction, *rEF* reduced ejection fraction, *RVEF* right ventricular ejection fraction, *Tx* treatment, *w* weighted, *w/* with, *w/o* without

[a] AC dose reflects cumulative dosage. For those receiving chest radiation, dose is reported if available in article

[b] Longitudinal study

[c] Interval reflects time from initial chemotherapy

[d] The qualitative presence of edema was defined as having abnormal patchy areas of high T2w signal intensity. The quantitative presence of edema was defined as having a myocardium signal intensity normalized to skeletal muscle that was ≥2

[e] MACE reflects composite of CV death, appropriate ICD therapy, admission for decompensated heart failure

Table 3 Clinical studies using CMR to investigate anthracycline-associated myocardial remodeling

Author	Population (*N*, age, Ca)	Treatment[a] (mg/m^2 or Gy)	Time interval[c]	CMR	Findings
Choteni-mitkhun et al., 2015 [38]	$n = 51$ 48 ± 2 years Breast Ca, leukemia, lymphoma	Statin: 193 ± 27 No statin: 193 ± 15	6 m	• Function • Deformation	GOAL: Assess whether statins during AC tx can mitigate LVEF decline. • Statin: LVEF unchanged at 6 m after adjustment for confounders ($p = 0.03$); less decrease in GCS ($p > 0.05$) • Non-statin: LVEF decline by 6.5 % ± 1.5 % ($p = 0.03$)
Drafts et al., 2013 [48] [b]	$n = 53$ 50 ± 2 years Breast, MDS Leukemia, Lymphoma	50–375 #DOX equivalent	1, 3, 6 m	• Function • Deformation • Fibrosis (LGE)	GOAL: Longitudinal assessment at baseline, 1, 3, and 6 m post low to moderate dose AC • ↓LVEF, ↓GCS, ↑ PWV at 6 m from baseline ($p < 0.001$); PWV not correlated with cumulative AC dose ($p = 0.6$) or LVEF ($p = 0.64$) • Use of trastuzumab was not associated with larger decrement in LVEF or ↑PWV or worse strain
Tham et al., 2013 [60]	$n = 30$ 15.2 ± 2.7 years Lymphomas Other tumors	197.2 ± 84.3 Chest radiation, unspecified dose	7.6 ± 4.5 years	• Function • Edema (black blood T2 mapping) • Fibrosis (T1 mapping (SASHA)) • Fibrosis (LGE)	GOAL: Cross-sectional description of diffuse fibrosis and aerobic exercise capacity in childhood cancer survivors • Normal mean LVEF (57.6 ± 4.9 %, range 41–74 %) • ECV positively correlated with AC dose($r = 0.40$, $p = 0.036$); inversely correlated to peak VO2max ($r = -0.52$, $p = 0.005$), LV wall thickness to height ratio ($r = -0.72$, $p < 0.001$), LV mass to volume ratio ($r = -0.64$)($p < 0.001$) • No edema by T2; T2 not correlated with T1 values or ECV, but inversely correlated with AC dose and peak VO2max ($r = -0.49$, $p = 0.01$); no LGE in all subjects
Neilan et al., 2013 [61]	$n = 42$; $n = 14$ (rEF) 55 ± 17 years Lymphoma Breast cancer Leukemia, bone Ca	AC-pEF: 272 ± 59 AC-rEF: 301 ± 72 Chest radiation, unspecified dose	89 ± 40 m	• Function • Edema (T2w) • Fibrosis (T1 imaging (LL)) • Fibrosis (LGE)	GOAL: Cross-sectional assessment of diffuse fibrosis in adult cancer survivors • LVEF: pEF grp had EF 58 ± 8, rEF grp had 38 ± 8, all vs. control, $p = 0.004$; pEF vs. rEF, $p < 0.001$ • RVEF: lowest in rEF grp (39 ± 15 %, $p = 0.04$) • ECV: highest in patients with rEF vs. pEF, $p < 0.05$ • T2: no qualitative or quantitative evidence of edema[d]; LGE seen in 3 patients (rEF $n = 2$, pEF $n = 1$)
Jordan et al., 2014 [62] [b]	$n = 65$; $n = 42$ (chemo naive) 51 ± 12 years Breast Ca Leukemia, lymphoma	240 ± 85 #DOX equivalent 31 ± 20 Gy	3 months	• Function • Edema (T2w) • Fibrosis (Pre- and post-contrast T1) • Fibrosis (LGE-SI)	GOAL: Assess LV function, Δ in T1 mapping, T2 weighted, and LGE-SI pre- and 3 months post-chemo • Baseline: lower LVEF in group with prior chemo vs. no chemo (59 ± 6 % vs. 55 ± 6 %, $p = 0.007$). No difference in T2w relative enhancement ($p = 0.44$) or % edema ($p = 0.95$) • 3 m post-chemo: ↓ LVEF from 57 ± 6 % to 54 ± 7 % ($p < 0.001$, $n = 60$) with ↑ LGE-SI from 14.1 ± 5.1 to 15.9 ± 6.8 ($p < 0.05$); No Δ T2w edema ($p = 0.17$), or %edema ($p = 0.70$). No Δ pre- or post-contrast T1
Lunning et al., 2015 [69] [b]	$n = 10$ 59.6 ± 5.7 years Lymphomas	DOX 300	0, 3 m	• Function • Deformation (FT) • Fibrosis (LGE)	GOAL: Longitudinally assess ΔLVEF, deformation, fibrosis at baseline & after 3 m of DOX • Post-tx LVEF decrease ≥10 % in 5 patients ($p = 0.004$) • Pre-tx and post-tx GRS were lower compared to controls ($p < 0.01$) • Post-tx GCS lower than pre-tx ($p = 0.018$); both post-tx GCS and GLS were lower compared to controls ($p = 0.046$ and $p = 0.035$, respectively). • Positive LGE: new ($n = 1$), progressive ($n = 2$) segment
Toro-Salazar et al., 2013 [86]	$n = 46$ 22 years (12–42) y Leukemia	328 (200–600) Chest radiation, unspecified low dose	9.6 years (2.5–26.9)	• Function • Deformation • Fibrosis (T1 map (MLLSR))	GOAL: Cross-sectional analysis of childhood cancer survivors • ↑ LVEF compared to controls ($p < 0.01$), but within normal threshold ≥55 % • Deformation: $n = 45$ with reduced GCS ($p < 0.001$) and GLS ($p < 0.001$)

Table 3 (continued)

Author	Population (*N*, age, Ca)	Treatment[a] (mg/m^2 or Gy)	Time interval[c]	CMR	Findings
	Lymphoma Other tumors			• Fibrosis (LGE)	• Lower 20-min post-contrast T1 values ($p = 0.01$) compared to control subjects • ECV: $n = 5$ of 27 with elevated ECV (0.38 ± 0.07); none with LGE

Unless otherwise noted, age is reported as mean ± standard deviation at time of visit. For studies with multiple types of AC, DOX equivalent dosage is reported when available and noted (#)

AC anthracycline, *DOX* doxorubicin, *ECV* myocardial extracellular volume, *FT* feature tracking, *GCS* global circumferential strain, *GLS* global longitudinal strain, *GRS* global radial strain, *LGE* late gadolinium enhancement, *LL* Look-Locker, *LVEF* left ventricular ejection fraction, *pEF* preserved ejection fraction, *PWV* pulse wave velocity, *SI* signal intensity, *rEF* reduced ejection fraction, *RVEF* right ventricular ejection fraction, *Tx* treatment, *w* weighted, *w/* with, *w/o* without

[a] AC dose reflects cumulative dosage. For those receiving chest radiation, dose is reported if available in article

[b] Longitudinal study

[c] Interval reflects time from initial chemotherapy

[d] The qualitative presence of edema was defined as having abnormal patchy areas of high T2w signal intensity. The quantitative presence of edema was defined as having a myocardium signal intensity normalized to skeletal muscle that was ≥2

in myocardial infarction is LGE imaging, while diffuse fibrosis imaging relies on T1 mapping.

The principle behind LGE imaging is that the "wash-in" and "wash-out" kinetics of GBCAs in normal myocardium is rapid, but in cases of acute myocyte cell membrane disruption or "scarred, fibrotic" tissue, the "wash-out" phase requires more time to complete. The delayed clearance of gadolinium from the extracellular space results in increased gadolinium concentration, which is reflected as a bright signal relative to normal myocardium that is nulled [64, 65]. Typically, images are acquired 10–20 min after a 0.1–0.2 mmol/kg GBCA bolus injection with the inversion time selected to suppress the signal in the native myocardium (i.e., "nulling" of the myocardium which reflects the return of proton spins to the zero point, dark appearance) (Fig. 2c). Of the various pulses sequences available for LGE imaging, inversion recovery (IR) and phase-sensitive inversion recovery (PSIR) with ECG-gated segmented gradient echo readout are widely used and provide the best contrast-to-noise ratio and contrast-enhancement-ratio [66, 67]. LGE can also be acquired using a PSIR with single shot bSSFP readout for multi-slice coverage [68]. This latter technique is useful in patients unable to perform multiple breath-holds or lay flat for a prolonged period of time. LGE can quantify focal regions of myocardial fibrosis as small as 0.16 g [64]. The extent of scaring can provide prognostic information while the scar pattern, when visualized early in the disease process, can provide insight into the underlying causes of the myopathy.

Findings of LGE in cases of AC exposure, however, are few and have only been described in limited studies [35, 37, 61, 69, 70] (Tables 2 and 3). The described patterns are atypical (including mid-myocardial, RV insertion point, epicardial, subendocardial, basal distribution), suggesting patchy myocarditis. A greater frequency of LGE has been reported in studies with combined AC and trastuzumab exposure [71–73] than in studies with AC alone. However, the true incidence and prevalence of focal versus diffuse interstitial fibrosis in AC-induced myocardial remodeling remains unclear. The challenge of LGE imaging is in detecting diffuse fibrosis [64, 65, 74, 75], which appears to be a more widely reported phenomenon in AC exposure (Table 3) and potentially reversible with existing therapeutics. The signal intensities in diffuse fibrosis may be completely nulled due to its isointense signal and appear similar to "normal" myocardial tissue on LGE imaging. In these cases, T1 mapping is better at differentiating diffuse fibrosis from normal tissue and correlate well with histologic findings of myocardial interstitial fibrosis [76].

In T1 mapping, multiple images are acquired with different T1 weightings. The signal intensities on the images are "fitted" to an equation for T1 relaxation in order to determine the T1 relaxation time for a region of interest, myocardial segment, or per pixel basis to generate a "map" whereby each

pixel intensity represents a specific T1 relaxation time (Fig. 2d). As an index, T1 mapping holds value because of its ability to detect interstitial myocardial fibrosis, which has been shown to affect mechanical behavior of the myocardium, precedes irreversible replacement fibrosis [77••], and can potentially be reversible with appropriate therapy [63, 78, 79]. Further, T1-based measures have been validated in many diffuse myocardial disease states and are shown to carry prognostic value in non-ischemic cardiomyopathies [80••]. There are many techniques for T1 mapping, which can be grouped as "inversion recovery," "saturation recovery," or hybrid [80••]. Inversion recovery techniques are more precise while saturation techniques are more accurate with each having their own limitations [80••, 81•, 82••] and hence, the importance of discussing institution-specific protocols and interpretation with local imagers specialized in CMR. Of these techniques, modified Look-Locker inversion recovery (MOLLI) [83] is most widely used and validated.

When gadolinium-based contrast agents (GBCAs) are used, the tissue relaxation properties change and often times T1 maps are acquired pre- and post-contrast injection (Fig. 2d). The difference between pre- and post-contrast T1 values corrected for by the patient's hematocrit, allows quantification of the extracellular volume fraction (ECV) [74, 75] (Fig. 2e). An increase in the ECV reflects expansion of the extracellular compartment. Because the ECV circumvents some of the confounders associated with T1-weighted imaging and T1 maps, an age- and sex-adjusted normal reference range can be established to discriminate between disease types and without the need for invasive endomyocardial biopsy [74, 75, 84, 85]. The ECV values should be interpreted in the context of age and sex, especially when measured cross-sectionally. Further, while accuracy and precision may vary with T1 mapping techniques and ECV values may differ between the sequences used, the reproducibility, however, is similar [81•] (Fig. 2e).

Several CMR-based clinical investigations have leveraged T1 mapping to study myocardial remodeling in cancer patients and survivors (Table 3). In one study of childhood cancer survivors [60] whereby the relationship between ECV, overall cardiac function, and aerobic exercise capacity (peak VO2max) was assessed, an increased ECV was directly correlated with higher AC dose ($r = 0.40$). The ECV was also associated with decreased mass/volume ratio ($r = -0.64$, a reflection of wall thinning) and lower peak VO2max ($r = -0.52$) despite having normal LVEF. In adult cancer survivors [61], the ECV had a positive association with the left atrial volume index ($r = 0.65$, $p < 0.001$) and a negative association with diastolic function ($r = -0.64$, $p < 0.001$ using lateral E′). Furthermore, the ECV was increased in those with a reduced ejection fraction compared to those with a preserved ejection fraction (ECV 0.38 ± 0.03 vs. 0.36 ± 0.02, $p < 0.03$). A separate study [86] found that post-gadolinium T1 values at 20 min were significantly correlated with increased end-systolic fiber stress (indicator of LV wall stress) and low LV mass index ($r = 0.52$, $p < 0.001$), which supports the findings by Neilan et al. [34] where LV mass index was found to be predictive of MACE. The ECV, however, was only weakly associated with fiber stress ($r = 0.369$, $p = 0.049$). Overall, the challenge in these studies, however, is the heterogeneity of the study cohorts (i.e., AC, AC + radiation) and many were cross-sectional in design.

Myocardial Perfusion Imaging for Epicardial Coronary and Microvascular Disease

Stress perfusion imaging measures the myocardial perfusion reserve (MPR), which is an indirect surrogate for coronary flow reserve (CFR) and is often assumed to only reflect the coronary circulation. Many clinicians associate stress perfusion imaging with epicardial coronary disease. However, the health of the microcirculation is also reflected by the MPR. In fact, of the total ~45-mL of coronary blood volume [87], 90 % resides in the microcirculation (i.e., the myocardial blood volume) and constitutes ~8 % of the LV mass [88]. MPR reflects the coronary circulation's capacity to increase blood flow when the perfusion bed is maximally dilated. Measurement is required during rest and at maximal vasodilation. In the healthy circulation, MPR and CFR are typically comparable. However, when there is coronary disease, regional (i.e., vessel specific) impairment of the MPR can be observed [89]. In cases of microvascular disease where there is lower capillary density (e.g., myocardial infarction, hypertension, diabetes, HFpEF), decreased MPR can be present in the absence of coronary stenosis, which may be the case with AC exposure. For those who have received combined AC and chest radiation, the presence of both accelerated epicardial and microvascular disease are plausible. Although nuclear stress perfusion with single photon emission computed tomography (SPECT) is frequently performed at the expense of radiation, recent findings from the Clinical Evaluation of Magnetic Resonance Imaging in Coronary heart disease (CE-MARC) trial suggest that perfusion CMR is superior [90] and more sensitive than SPECT in both women and men [91•]. Further, stress CMR is cost-effective for the evaluation of coronary disease [92].

Stress CMR is performed pharmacologically with an intravenous vasodilator (regadenoson, adenosine, or dipyridamole) [93] or inotropic agent (dobutamine) and at select institutions, exercise stress CMR [94] can also be performed. Stress perfusion CMR typically uses a T1-weighted, ECG-gated, single shot, 2D sequence [89]. These techniques measure the contrast enhancement (0.03–0.1 mmol/kg bolus injection at 3–5 ml/s) during the first pass of the contrast through the cardiac chambers and myocardium at rest and with stress. The myocardial

perfusion results can then be qualitatively or quantitatively assessed. With 2D CMR, dobutamine stress is more specific (86 %, 95 % CI 81–91 %) while vasodilator perfusion is more sensitive (91 %, 95 % CI 88–94 %) for detection of epicardial coronary disease [95]. 3D CMR improves both sensitivity and specificity (85 and 91 %, respectively) compared to fractional flow reserve measurements (77 and 95 %, respectively) [96].

Although there is high potential benefit for using stress CMR to interrogate the myocardial microcirculation of cancer survivors as demonstrated in other disease states [97, 98], few studies have used stress CMR. To date, only one study has used dobutamine stress CMR in the setting of a 4-month exercise intervention [99] while another used rest first-pass perfusion CMR [70] in a 2-year longitudinal study (CMR at baseline, 1 year, 2 years post-AC). The study using dobutamine stress CMR in adult breast cancer survivors (age 53 ± 7 years) concluded that the LV volumetry increased while EF decreased post-exercise intervention ($p < 0.05$) despite exercise therapy during chemotherapy [99]. The dobutamine-induced peak LVEF decreased at 4 months (pre-intervention 79 ± 4 vs. 76 ± 6 % post), but was not statistically significant ($p = 0.087$). There was no significant change in post-intervention dobutamine-induced peak heart rate or oxygen consumption from baseline. Regional wall motion abnormalities were not reported. On the other hand, the rest perfusion study [70] in survivors of childhood cancer receiving both AC and chest radiation concluded that there were abnormal rest first-pass perfusion defects (predominantly transmural) in multiple distributions (mostly septal and inferior wall) at baseline and longitudinally. At 1 year, new rest defects were seen in 11 of 49 patients who had normal baseline scans ($p < 0.05$) while 12 of 14 had persistent defects. At 2 years, new rest defects were seen in 9 of 34 patients who had normal baseline scans ($p < 0.05$) while 12 continued to have persistent defects from baseline. Stress perfusion was not performed and the severity of the defect was not reported. While there were patients who reportedly had new rest perfusion defects and some had persistent defects over the course of a 2-year period, one could not ascertain (1) whether the rest defects are true defects in the absence of stress perfusion images or (2) whether the severity of the defects increased over time. These studies should be interpreted in light of the following limitations: (1) small sample size, (2) the presence of dark-rim artifacts due to Gibbs ringing are frequent in the septum and interpretation is aided when stress images are available, and (3) perfusion CMR with a stress agent is vital for assessment of MPR—as with all perfusion scans, rest defects without the correlative stress images are challenging to interpret. Because of these limitations, it is difficult to demonstrate the true utility of stress CMR in this specific population. However, given the positive supporting data for stress perfusion CMR in large studies of epicardial coronary disease, future well-designed clinical studies leveraging this technology would enhance our understanding of AC-associated myocardial remodeling and the microcirculation.

Conclusion

As a comprehensive CV imaging technique, CMR has added value in characterizing myocardial remodeling. However, it is important to note that CMR protocols and use of pulse sequences vary among institutions and vendor platforms. Therefore, clinicians and imagers need to work closely to establish standardized protocols and reference ranges. Although early detection of morphologic, functional, and microvascular changes can potentially be targeted for preventive therapy, additional investigations using standardized CMR techniques are needed to validate published preliminary findings. As cancer therapy improves, survivors will have a longer lifespan and many will face unanticipated consequences of cancer treatment. Mitigation of short and long-term CV side effects from cancer treatment may be facilitated through the incorporation of CMR for comprehensive assessment of myocardial health.

Acknowledgments This work is supported by pilot grants from the UCLA Jonsson Comprehensive Cancer Foundation and UCLA CTSI grant UL1TR000124.

Compliance with Ethical Standards

Conflict of Interest Kim-Lien Nguyen, Peng Hu, Daniel B. Ennis, Jiaxin Shao, Kimberly A. Pham, and Joseph J. Chen declare that they have no conflict of interest.

Human and Animal Rights and Informed Consent This article does not contain any studies with human or animal subjects performed by any of the authors.

References

Papers of particular interest, published recently, have been highlighted as:
- • Of importance
- •• Of major importance

1.•• Lancellotti P, Nkomo VT, Badano LP, Bergler-Klein J, Bogaert J, Davin L, et al. Expert consensus for multi-modality imaging evaluation of cardiovascular complications of radiotherapy in adults: a report from the European Association of Cardiovascular Imaging and the American Society of Echocardiography. Eur Heart J Cardiovasc Imag. 2013;14(8):721–40. doi:10.1093/ehjci/jet123. **Discusses cardiovascular complications of radiotherapy and follow-up imaging.**

2. Vejpongsa P, Yeh ET. Prevention of anthracycline-induced cardiotoxicity: challenges and opportunities. J Am Coll Cardiol. 2014;64(9):938–45. doi:10.1016/j.jacc.2014.06.1167.
3.• Nikitovic D, Juranek I, Wilks MF, Tzardi M, Tsatsakis A, Tzanakakis GN. Anthracycline-dependent cardiotoxicity and extracellular matrix remodeling. Chest. 2014;146(4):1123–30. doi:10.1378/chest.14-0460. **Outlines molecular basis for extracellular matrix remodeling.**
4. D'Amore C, Gargiulo P, Paolillo S, Pellegrino AM, Formisano T, Mariniello A, et al. Nuclear imaging in detection and monitoring of cardiotoxicity. World J Radiol. 2014;6(7):486–92. doi:10.4329/wjr.v6.i7.486.
5. Curigliano G, Cardinale D, Suter T, Plataniotis G, de Azambuja E, Sandri MT, et al. Cardiovascular toxicity induced by chemotherapy, targeted agents and radiotherapy: ESMO Clinical Practice Guidelines. Annal Oncol Offic J Eur Soc Med Oncol / ESMO. 2012;23 Suppl 7:vii155–66. doi:10.1093/annonc/mds293.
6. Hunt SA, Abraham WT, Chin MH, Feldman AM, Francis GS, Ganiats TG, et al. 2009 focused update incorporated into the ACC/AHA 2005 Guidelines for the Diagnosis and Management of Heart Failure in Adults: a report of the American College of Cardiology Foundation/American Heart Association Task Force on Practice Guidelines: developed in collaboration with the International Society for Heart and Lung Transplantation. Circulation. 2009;119(14):e391–479. doi:10.1161/circulationaha.109.192065.
7. Billingham ME, Mason JW, Bristow MR, Daniels JR. Anthracycline cardiomyopathy monitored by morphologic changes. Cancer Treat Rep. 1978;62(6):865–72.
8. Ferrans VJ. Overview of cardiac pathology in relation to anthracycline cardiotoxicity. Cancer Treat Rep. 1978;62(6):955–61.
9. Bernaba BN, Chan JB, Lai CK, Fishbein MC. Pathology of late-onset anthracycline cardiomyopathy. Cardiovascul Pathol Offic J Soc Cardiovasc Pathol. 2010;19(5):308–11. doi:10.1016/j.carpath.2009.07.004.
10. Lefrak EA, Pitha J, Rosenheim S, Gottlieb JA. A clinicopathologic analysis of adriamycin cardiotoxicity. Cancer. 1973;32(2):302–14.
11. Yeh ET, Bickford CL. Cardiovascular complications of cancer therapy: incidence, pathogenesis, diagnosis, and management. J Am Coll Cardiol. 2009;53(24):2231–47. doi:10.1016/j.jacc.2009.02.050.
12. Wouters KA, Kremer LC, Miller TL, Herman EH, Lipshultz SE. Protecting against anthracycline-induced myocardial damage: a review of the most promising strategies. Br J Haematol. 2005;131(5):561–78. doi:10.1111/j.1365-2141.2005.05759.x.
13. Bayram C, Cetin I, Tavil B, Yarali N, Ekici F, Isik P, et al. Evaluation of cardiotoxicity by tissue Doppler imaging in childhood leukemia survivors treated with low-dose anthracycline. Pediatr Cardiol. 2015;36(4):862–6. doi:10.1007/s00246-015-1096-6.
14.•• Armenian SH, Hudson MM, Mulder RL, Chen MH, Constine LS, Dwyer M, et al. Recommendations for cardiomyopathy surveillance for survivors of childhood cancer: a report from the International Late Effects of Childhood Cancer Guideline Harmonization Group. Lancet Oncol. 2015;16(3):e123–36. doi:10.1016/s1470-2045(14)70409-7. **This paper provides consensus among multiple guidelines on cardiomyopathy surveillance of childhood cancer survivors.**
15. Hequet O, Le QH, Moullet I, Pauli E, Salles G, Espinouse D, et al. Subclinical late cardiomyopathy after doxorubicin therapy for lymphoma in adults. J Clin Oncol Offic J Am Soc. 2004;22(10):1864–71. doi:10.1200/jco.2004.06.033.
16. Frangogiannis NG. Matricellular proteins in cardiac adaptation and disease. Physiol Rev. 2012;92(2):635–88. doi:10.1152/physrev.00008.2011.
17. Harvey PA, Leinwand LA. The cell biology of disease: cellular mechanisms of cardiomyopathy. J Cell Biol. 2011;194(3):355–65. doi:10.1083/jcb.201101100.
18. Janicki JS, Brower GL, Gardner JD, Chancey AL, Stewart Jr JA. The dynamic interaction between matrix metalloproteinase activity and adverse myocardial remodeling. Heart Fail Rev. 2004;9(1):33–42. doi:10.1023/B:HREV.0000011392.03037.7e.
19. Zhang S, Liu X, Bawa-Khalfe T, Lu LS, Lyu YL, Liu LF, et al. Identification of the molecular basis of doxorubicin-induced cardiotoxicity. Nat Med. 2012;18(11):1639–42. doi:10.1038/nm.2919.
20. Smith LA, Cornelius VR, Plummer CJ, Levitt G, Verrill M, Canney P, et al. Cardiotoxicity of anthracycline agents for the treatment of cancer: systematic review and meta-analysis of randomised controlled trials. BMC Cancer. 2010;10:337. doi:10.1186/1471-2407-10-337.
21. Gajarsa JJ, Kloner RA. Left ventricular remodeling in the post-infarction heart: a review of cellular, molecular mechanisms, and therapeutic modalities. Heart Fail Rev. 2011;16(1):13–21. doi:10.1007/s10741-010-9181-7.
22. Ridgway JP. Cardiovascular magnetic resonance physics for clinicians: part I. J Cardiovasc Magn Reson. 2010;12:71. doi:10.1186/1532-429X-12-71.
23. Pfeiffer MP, Biederman RW. Cardiac MRI: a general overview with emphasis on current use and indications. Med Clin North Am. 2015;99(4):849–61. doi:10.1016/j.mcna.2015.02.011.
24. Kramer CM, Barkhausen J, Flamm SD, Kim RJ, Nagel E. Standardized cardiovascular magnetic resonance (CMR) protocols 2013 update. J Cardiovasc Magn Reson. 2013;15:91. doi:10.1186/1532-429x-15-91.
25. Finn JP, Nael K, Deshpande V, Ratib O, Laub G. Cardiac MR imaging: state of the technology. Radiology. 2006;241(2):338–54. doi:10.1148/radiol.2412041866.
26. Carr JC, Simonetti O, Bundy J, Li D, Pereles S, Finn JP. Cine MR angiography of the heart with segmented true fast imaging with steady-state precession. Radiology. 2001;219(3):828–34. doi:10.1148/radiology.219.3.r01jn44828.
27. Michaely HJ, Nael K, Schoenberg SO, Laub G, Reiser MF, Finn JP, et al. Analysis of cardiac function–comparison between 1.5 Tesla and 3.0 Tesla cardiac cine magnetic resonance imaging: preliminary experience. Invest Radiol. vol 2. United States2006. p. 133–40.
28. Miller S, Simonetti OP, Carr J, Kramer U, Finn JP. MR Imaging of the heart with cine true fast imaging with steady-state precession: influence of spatial and temporal resolutions on left ventricular functional parameters. Radiology. 2002;223(1):263–9. doi:10.1148/radiol.2231010235.
29. Gulati G, Zhang KW, Scherrer-Crosbie M, Ky B. Cancer and cardiovascular disease: the use of novel echocardiography measures to predict subsequent cardiotoxicity in breast cancer treated with anthracyclines and trastuzumab. Curr Heart Fail Rep. 2014;11(4):366–73. doi:10.1007/s11897-014-0214-8.
30. Armstrong GT, Plana JC, Zhang N, Srivastava D, Green DM, Ness KK, et al. Screening adult survivors of childhood cancer for cardiomyopathy: comparison of echocardiography and cardiac magnetic resonance imaging. J Clin Oncol Offic J Am Soc. 2012;30(23):2876–84. doi:10.1200/jco.2011.40.3584.
31. Toro-Salazar OH, Ferranti J, Lorenzoni R, Walling S, Mazur W, Raman SV, et al. Feasibility of echocardiographic techniques to detect subclinical cancer therapeutics-related cardiac dysfunction among high-dose patients when compared with cardiac magnetic resonance imaging. J Am Soc Echocardiograph Offic Pub. 2016;29(2):119–31. doi:10.1016/j.echo.2015.10.008.
32. Grothues F, Moon JC, Bellenger NG, Smith GS, Klein HU, Pennell DJ. Interstudy reproducibility of right ventricular volumes, function, and mass with cardiovascular magnetic

resonance. Am Heart J. 2004;147(2):218–23. doi:10.1016/j.ahj.2003.10.005.

33. Grothues F, Smith GC, Moon JC, Bellenger NG, Collins P, Klein HU, et al. Comparison of interstudy reproducibility of cardiovascular magnetic resonance with two-dimensional echocardiography in normal subjects and in patients with heart failure or left ventricular hypertrophy. Am J Cardiol. 2002;90(1):29–34.
34. Ylanen K, Poutanen T, Savikurki-Heikkila P, Rinta-Kiikka I, Eerola A, Vettenranta K. Cardiac magnetic resonance imaging in the evaluation of the late effects of anthracyclines among long-term survivors of childhood cancer. J Am Coll Cardiol. 2013;61(14):1539–47. doi:10.1016/j.jacc.2013.01.019.
35. Cheung YF, Lam WW, Ip JJ, Cheuk DK, Cheng FW, Yang JY, et al. Myocardial iron load and fibrosis in long term survivors of childhood leukemia. Pediatr Blood Cancer. 2015;62(4):698–703. doi:10.1002/pbc.25369.
36. Grover S, Lou PW, Bradbrook C, Cheong K, Kotasek D, Leong DP, et al. Early and late changes in markers of aortic stiffness with breast cancer therapy. Intern Med J. 2015;45(2):140–7. doi:10.1111/imj.12645.
37. Neilan TG, Coelho-Filho OR, Pena-Herrera D, Shah RV, Jerosch-Herold M, Francis SA, et al. Left ventricular mass in patients with a cardiomyopathy after treatment with anthracyclines. Am J Cardiol. 2012;110(11):1679–86. doi:10.1016/j.amjcard.2012.07.040.
38. Chotenimitkhun R, D'Agostino Jr R, Lawrence JA, Hamilton CA, Jordan JH, Vasu S, et al. Chronic statin administration may attenuate early anthracycline-associated declines in left ventricular ejection function. Can J Cardiol. 2015;31(3):302–7. doi:10.1016/j.cjca.2014.11.020.
39. Cardinale D, Colombo A, Lamantia G, Colombo N, Civelli M, De Giacomi G, et al. Anthracycline-induced cardiomyopathy: clinical relevance and response to pharmacologic therapy. J Am Coll Cardiol. 2010;55(3):213–20. doi:10.1016/j.jacc.2009.03.095.
40. Hundley WG, Bluemke DA, Finn JP, Flamm SD, Fogel MA, Friedrich MG, et al. ACCF/ACR/AHA/NASCI/SCMR 2010 expert consensus document on cardiovascular magnetic resonance: a report of the American College of Cardiology Foundation Task Force on Expert Consensus Documents. J Am Coll Cardiol. 2010;55(23):2614–62. doi:10.1016/j.jacc.2009.11.011.
41.•• Plana JC, Galderisi M, Barac A, Ewer MS, Ky B, Scherrer-Crosbie M, et al. Expert consensus for multimodality imaging evaluation of adult patients during and after cancer therapy: a report from the American Society of Echocardiography and the European Association of Cardiovascular Imaging. Eur Heart J Cardiovasc Imag. 2014;15(10):1063–93. doi:10.1093/ehjci/jeu192. **Outlines intersociety recommendations for imaging of adult cancer patients and survivors.**
42. Shehata ML, Cheng S, Osman NF, Bluemke DA, Lima JA. Myocardial tissue tagging with cardiovascular magnetic resonance. J Cardiovasc Magn Reson. 2009;11:55. doi:10.1186/1532-429x-11-55.
43. Axel L, Dougherty L. MR imaging of motion with spatial modulation of magnetization. Radiology. 1989;171(3):841–5. doi:10.1148/radiology.171.3.2717762.
44. Moghaddam AN, Natsuaki Y, Finn J. CMR Tagging in the polar coordinate system. Annual Society of Cardiovascular Magnetic Resonance 2011 Meeting; February 2, 2011.
45. Wang Z, Nasiraei-Moghaddam A, Reyhan ML, Srinivasan S, Finn JP, Ennis DB. Complementary radial tagging for improved myocardial tagging contrast. Magnet Reson Med Offic J Soc Magnet. 2015;73(4):1432–40. doi:10.1002/mrm.25259.
46. Hor KN, Baumann R, Pedrizzetti G, Tonti G, Gottliebson WM, Taylor M, et al. Magnetic resonance derived myocardial strain assessment using feature tracking. J Visual Exp JoVE. 2011(48). doi:10.3791/2356.
47. Hor KN, Gottliebson WM, Carson C, Wash E, Cnota J, Fleck R, et al. Comparison of magnetic resonance feature tracking for strain calculation with harmonic phase imaging analysis. JACC Cardiovasc Imaging. 2010;3(2):144–51. doi:10.1016/j.jcmg.2009.11.006.
48. Drafts BC, Twomley KM, D'Agostino Jr R, Lawrence J, Avis N, Ellis LR, et al. Low to moderate dose anthracycline-based chemotherapy is associated with early noninvasive imaging evidence of subclinical cardiovascular disease. JACC Cardiovasc Imaging. 2013;6(8):877–85. doi:10.1016/j.jcmg.2012.11.017.
49. Scholz TD, Fleagle SR, Burns TL, Skorton DJ. Tissue determinants of nuclear magnetic resonance relaxation times. Effect of water and collagen content in muscle and tendon. Invest Radiol. 1989;24(11):893–8.
50. Higgins CB, Herfkens R, Lipton MJ, Sievers R, Sheldon P, Kaufman L, et al. Nuclear magnetic resonance imaging of acute myocardial infarction in dogs: alterations in magnetic relaxation times. Am J Cardiol. 1983;52(1):184–8.
51. Simonetti OP, Finn JP, White RD, Laub G, Henry DA. "Black blood" T2-weighted inversion-recovery MR imaging of the heart. Radiology. 1996;199(1):49–57. doi:10.1148/radiology.199.1.8633172.
52. Payne AR, Casey M, McClure J, McGeoch R, Murphy A, Woodward R, et al. Bright-blood T2-weighted MRI has higher diagnostic accuracy than dark-blood short tau inversion recovery MRI for detection of acute myocardial infarction and for assessment of the ischemic area at risk and myocardial salvage. Circ Cardiovasc Imaging. 2011;4(3):210–9. doi:10.1161/circimaging.110.960450.
53. Kellman P, Aletras AH, Mancini C, McVeigh ER, Arai AE. T2-prepared SSFP improves diagnostic confidence in edema imaging in acute myocardial infarction compared to turbo spin echo. Magnet Reson Med Offic J Soc Magnet. 2007;57(5):891–7. doi:10.1002/mrm.21215.
54. Giri S, Chung YC, Merchant A, Mihai G, Rajagopalan S, Raman SV, et al. T2 quantification for improved detection of myocardial edema. J Cardiovasc Magn Reson. 2009;11:56. doi:10.1186/1532-429x-11-56.
55. Thavendiranathan P, Walls M, Giri S, Verhaert D, Rajagopalan S, Moore S, et al. Improved detection of myocardial involvement in acute inflammatory cardiomyopathies using T2 mapping. Circ Cardiovasc Imaging. 2012;5(1):102–10. doi:10.1161/circimaging.111.967836.
56. McAlindon EJ, Pufulete M, Harris JM, Lawton CB, Moon JC, Manghat N, et al. Measurement of myocardium at risk with cardiovascular MR: comparison of techniques for edema imaging. Radiology. 2015;275(1):61–70. doi:10.1148/radiol.14131980.
57. Abdel-Aty H, Boye P, Zagrosek A, Wassmuth R, Kumar A, Messroghli D, et al. Diagnostic performance of cardiovascular magnetic resonance in patients with suspected acute myocarditis: comparison of different approaches. J Am Coll Cardiol. 2005;45(11):1815–22. doi:10.1016/j.jacc.2004.11.069.
58. Nassenstein K, Nensa F, Schlosser T, Bruder O, Umutlu L, Lauenstein T, et al. Cardiac MRI: T2-Mapping Versus T2-Weighted Dark-Blood TSE Imaging for Myocardial Edema Visualization in Acute Myocardial Infarction. RoFo Fortschritt Auf Dem Geb Rontgens Nuklearmed. 2014;186(2):166–72. doi:10.1055/s-0033-1350516.
59. Abdel-Aty H, Zagrosek A, Schulz-Menger J, Taylor AJ, Messroghli D, Kumar A, et al. Delayed enhancement and T2-weighted cardiovascular magnetic resonance imaging differentiate acute from chronic myocardial infarction. Circulation. 2004;109(20):2411–6. doi:10.1161/01.cir.0000127428.10985.c6.
60. Tham EB, Haykowsky MJ, Chow K, Spavor M, Kaneko S, Khoo NS, et al. Diffuse myocardial fibrosis by T1-mapping in children with subclinical anthracycline cardiotoxicity: relationship to

exercise capacity, cumulative dose and remodeling. J Cardiovasc Magn Reson. 2013;15:48. doi:10.1186/1532-429x-15-48.

61. Neilan TG, Coelho-Filho OR, Shah RV, Feng JH, Pena-Herrera D, Mandry D, et al. Myocardial extracellular volume by cardiac magnetic resonance imaging in patients treated with anthracycline-based chemotherapy. Am J Cardiol. 2013;111(5):717–22. doi:10.1016/j.amjcard.2012.11.022.
62. Jordan JH, D'Agostino Jr RB, Hamilton CA, Vasu S, Hall ME, Kitzman DW, et al. Longitudinal assessment of concurrent changes in left ventricular ejection fraction and left ventricular myocardial tissue characteristics after administration of cardiotoxic chemotherapies using T1-weighted and T2-weighted cardiovascular magnetic resonance. Circ Cardiovasc Imaging. 2014;7(6):872–9. doi:10.1161/circimaging.114.002217.
63. Mewton N, Liu CY, Croisille P, Bluemke D, Lima JA. Assessment of myocardial fibrosis with cardiovascular magnetic resonance. J Am Coll Cardiol. 2011;57(8):891–903. doi:10.1016/j.jacc.2010.11.013.
64. Doltra A, Amundsen BH, Gebker R, Fleck E, Kelle S. Emerging concepts for myocardial late gadolinium enhancement MRI. Curr Cardiol Rev. 2013;9(3):185–90.
65. Kellman P, Arai AE. Cardiac imaging techniques for physicians: late enhancement. J Magn Reson Imaging. 2012;36(3):529–42. doi:10.1002/jmri.23605.
66. Simonetti OP, Kim RJ, Fieno DS, Hillenbrand HB, Wu E, Bundy JM, et al. An improved MR imaging technique for the visualization of myocardial infarction. Radiology. 2001;218(1):215–23. doi:10.1148/radiology.218.1.r01ja50215.
67. Kellman P, Arai AE, McVeigh ER, Aletras AH. Phase-sensitive inversion recovery for detecting myocardial infarction using gadolinium-delayed hyperenhancement. Magnet Reson Med Offic J Soc Magnet. 2002;47(2):372–83.
68. Huber A, Hayes C, Spannagl B, Rieber J, Klauss V, Schoenberg SO, et al. Phase-sensitive inversion recovery single-shot balanced steady-state free precession for detection of myocardial infarction during a single breathhold. Acad Radiol. 2007;14(12):1500–8. doi:10.1016/j.acra.2007.06.017.
69. Lunning MA, Kutty S, Rome ET, Li L, Padiyath A, Loberiza F, et al. Cardiac magnetic resonance imaging for the assessment of the myocardium after doxorubicin-based chemotherapy. Am J Clin Oncol. 2015;38(4):377–81. doi:10.1097/COC.0b013e31829e19be.
70. de Ville de Goyet M, Brichard B, Robert A, Renard L, Veyckemans F, Vanhoutte L, et al. Prospective cardiac MRI for the analysis of biventricular function in children undergoing cancer treatments. Pediatr Blood Cancer. 2015;62(5):867–74. doi:10.1002/pbc.25381.
71. Fallah-Rad N, Lytwyn M, Fang T, Kirkpatrick I, Jassal DS. Delayed contrast enhancement cardiac magnetic resonance imaging in trastuzumab induced cardiomyopathy. J Cardiovasc Magn Reson. 2008;10:5. doi:10.1186/1532-429x-10-5.
72. Wadhwa D, Fallah-Rad N, Grenier D, Krahn M, Fang T, Ahmadie R, et al. Trastuzumab mediated cardiotoxicity in the setting of adjuvant chemotherapy for. Breast Cancer Res Treat. 2009;117(2):357–64. doi:10.1007/s10549-008-0260-6.
73. Lawley C, Wainwright C, Segelov E, Lynch J, Beith J, McCrohon J. Pilot study evaluating the role of cardiac magnetic resonance imaging in. Asia Pac J Clin Oncol. 2012;8(1):95–100. doi:10.1111/j.1743-7563.2011.01462.x.
74. Maestrini V, Treibel TA, White SK, Fontana M, Moon JC. T1 mapping for characterization of intracellular and extracellular myocardial diseases in heart failure. Curr Cardiovasc Imag Rep. 2014;7:9287. doi:10.1007/s12410-014-9287-8.
75. Ugander M, Oki AJ, Hsu LY, Kellman P, Greiser A, Aletras AH, et al. Extracellular volume imaging by magnetic resonance imaging provides insights into overt and sub-clinical myocardial pathology. Eur Heart J. 2012;33(10):1268–78. doi:10.1093/eurheartj/ehr481.
76. Sibley CT, Noureldin RA, Gai N, Nacif MS, Liu S, Turkbey EB, et al. T1 Mapping in cardiomyopathy at cardiac MR: comparison with endomyocardial biopsy. Radiology. 2012;265(3):724–32. doi:10.1148/radiol.12112721.
77.•• Donekal S, Venkatesh BA, Liu YC, Liu CY, Yoneyama K, Wu CO, et al. Interstitial fibrosis, left ventricular remodeling, and myocardial mechanical behavior in a population-based multiethnic cohort: the Multi-Ethnic Study of Atherosclerosis (MESA) study. Circ Cardiovasc Imaging. 2014;7(2):292–302. doi:10.1161/circimaging.113.001073. **This paper demonstrates the relationship between CMR measures of interstitial fibrosis and myocardial deformation.**
78. Brilla CG, Funck RC, Rupp H. Lisinopril-mediated regression of myocardial fibrosis in patients with hypertensive heart disease. Circulation. 2000;102(12):1388–93.
79. Diez J, Querejeta R, Lopez B, Gonzalez A, Larman M, Martinez Ubago JL. Losartan-dependent regression of myocardial fibrosis is associated with reduction of left ventricular chamber stiffness in hypertensive patients. Circulation. 2002;105(21):2512–7.
80.•• Taylor AJ, Salerno M, Dharmakumar R, Jerosch-Herold M. T1 mapping: basic techniques and clinical applications. JACC Cardiovasc Imaging. 2016;9(1):67–81. doi:10.1016/j.jcmg.2015.11.005. **This work summarizes the basics of T1 mapping and applications.**
81.• Roujol S, Weingartner S, Foppa M, Chow K, Kawaji K, Ngo LH, et al. Accuracy, precision, and reproducibility of four T1 mapping sequences: a head-to-head comparison of MOLLI, ShMOLLI, SASHA, and SAPPHIRE. Radiology. 2014;272(3):683–9. doi:10.1148/radiol.14140296. **MOLLI based techniques were more precise while saturation based techniques were more accurate.**
82.•• Kellman P, Hansen MS. T1-mapping in the heart: accuracy and precision. J Cardiovasc Magn Reson. 2014;16:2. doi:10.1186/1532-429x-16-2. **The importance of accuracy and precision as well as artifacts seen T1 mapping techniques are discussed.**
83. Messroghli DR, Radjenovic A, Kozerke S, Higgins DM, Sivananthan MU, Ridgway JP. Modified Look-Locker Inversion recovery (MOLLI) for high-resolution T1 mapping of the heart. Magnet Reson Med Offic J Soc Magnet. 2004;52(1):141–6. doi:10.1002/mrm.20110.
84. Sado DM, Flett AS, Banypersad SM, White SK, Maestrini V, Quarta G, et al. Cardiovascular magnetic resonance measurement of myocardial extracellular volume in health and disease. Heart. 2012;98(19):1436–41. doi:10.1136/heartjnl-2012-302346.
85. Liu CY, Liu YC, Wu C, Armstrong A, Volpe GJ, van der Geest RJ, et al. Evaluation of age-related interstitial myocardial fibrosis with cardiac magnetic resonance contrast-enhanced T1 mapping: MESA (Multi-Ethnic Study of Atherosclerosis). J Am Coll Cardiol. 2013;62(14):1280–7. doi:10.1016/j.jacc.2013.05.078.
86. Toro-Salazar OH, Gillan E, O'Loughlin MT, Burke GS, Ferranti J, Stainsby J, et al. Occult cardiotoxicity in childhood cancer survivors exposed to anthracycline therapy. Circ Cardiovasc Imaging. 2013;6(6):873–80. doi:10.1161/circimaging.113.000798.
87. Kassab GS, Fung YC. Topology and dimensions of pig coronary capillary network. Am J Physiol. 1994;267(1 Pt 2):H319–25.
88. Kaul S, Jayaweera AR. Coronary and myocardial blood volumes: noninvasive tools to assess the coronary microcirculation? Circulation. 1997;96(3):719–24.
89. Coelho-Filho OR, Rickers C, Kwong RY, Jerosch-Herold M. MR myocardial perfusion imaging. Radiology. 2013;266(3):701–15. doi:10.1148/radiol.12110918.
90. Greenwood JP, Maredia N, Younger JF, Brown JM, Nixon J, Everett CC, et al. Cardiovascular magnetic resonance and single-photon emission computed tomography for diagnosis of coronary

heart disease (CE-MARC): a prospective trial. Lancet. 2012;379(9814):453–60. doi:10.1016/s0140-6736(11)61335-4.

91.• Greenwood JP, Motwani M, Maredia N, Brown JM, Everett CC, Nixon J, et al. Comparison of cardiovascular magnetic resonance and single-photon emission computed tomography in women with suspected coronary artery disease from the Clinical Evaluation of Magnetic Resonance Imaging in Coronary Heart Disease (CE-MARC) Trial. Circulation. 2014;129(10):1129–38. doi:10.1161/circulationaha.112.000071. **This study demonstrated the superiority of stress perfusion CMR over SPECT for diagnosis of coronary artery disease.**

92. Walker S, Girardin F, McKenna C, Ball SG, Nixon J, Plein S, et al. Cost-effectiveness of cardiovascular magnetic resonance in the diagnosis of coronary heart disease: an economic evaluation using data from the CE-MARC study. Heart. 2013;99(12):873–81. doi:10.1136/heartjnl-2013-303624.

93. Nguyen KL, Bandettini WP, Shanbhag S, Leung SW, Wilson JR, Arai AE. Safety and tolerability of regadenoson CMR. Eur Heart J Cardiovasc Imag. 2014;15(7):753–60. doi:10.1093/ehjci/jet278.

94. Foster EL, Arnold JW, Jekic M, Bender JA, Balasubramanian V, Thavendiranathan P, et al. MR-compatible treadmill for exercise stress cardiac magnetic resonance imaging. Magnet Reson Med Offic J Soc Magnet. 2012;67(3):880–9. doi:10.1002/mrm.23059.

95. Nandalur KR, Dwamena BA, Choudhri AF, Nandalur MR, Carlos RC. Diagnostic performance of stress cardiac magnetic resonance imaging in the detection of coronary artery disease: a meta-analysis. J Am Coll Cardiol. 2007;50(14):1343–53. doi:10.1016/j.jacc.2007.06.030.

96. Manka R, Wissmann L, Gebker R, Jogiya R, Motwani M, Frick M, et al. Multicenter evaluation of dynamic three-dimensional magnetic resonance myocardial perfusion imaging for the detection of coronary artery disease defined by fractional flow reserve. Circulation Cardiovasc Imag. 2015;8(5). doi:10.1161/circimaging.114.003061.

97. Ismail TF, Hsu LY, Greve AM, Goncalves C, Jabbour A, Gulati A, et al. Coronary microvascular ischemia in hypertrophic cardiomyopathy—a pixel-wise quantitative cardiovascular magnetic resonance perfusion study. J Cardiovasc Magn Reson. 2014;16:49. doi:10.1186/s12968-014-0049-1.

98. Hsu LY, Groves DW, Aletras AH, Kellman P, Arai AE. A quantitative pixel-wise measurement of myocardial blood flow by contrast-enhanced first-pass CMR perfusion imaging: microsphere validation in dogs and feasibility study in humans. JACC Cardiovasc Imaging. 2012;5(2):154–66. doi:10.1016/j.jcmg.2011.07.013.

99. Haykowsky MJ, Mackey JR, Thompson RB, Jones LW, Paterson DI. Adjuvant trastuzumab induces ventricular remodeling despite aerobic exercise training. Clin Cancer Res. 2009;15(15):4963–7. doi:10.1158/1078-0432.CCR-09-0628.

100. Shao J, Nguyen KL, Natsuaki Y, Spottiswoode B, Hu P. Instantaneous signal loss simulation (InSiL): an improved algorithm for myocardial T(1) mapping using the MOLLI sequence. J Magn Reson Imaging. 2015;41(3):721–9. doi:10.1002/jmri.24599.